Table 2 Requirements of electromagnetic and acoustic methods on Earth for some liquid metals

Metal	B, Wb m^{-2}	$q_j \times 10^{-5}$, Wm^{-2}	t_m, s	$T \times 10^{-3}$, Nm	$\bar{P}_{lev}$, Case 1	$\bar{P}_{dr}$, Case 1	$\bar{P}_{lev}$, Case 2	$\bar{P}_{dr}$, Case 2
Copper	0.03	2.4	179	3	3	1.5	6.4	3.2
Aluminum	0.02	1.0	162	3	1.5	3.6	2.7	6.4
Callium	0.03	2.1	~0.5	3	2.5	3.2	2.5	3.2
Nickel	0.03	4.67	157	3	3	5	7.2	12

Table 3 Requirements of electromagnetic and acoustic methods in microgravity for some liquid metals

Metal	$B \times 10^{-5}$, Wb m^{-2}	q_j, W m^{-2}	t_m, s	$\bar{P}_{lev} \times 10^3$, Case 1	$\bar{P}_{lev} \times 10^3$, Case 2
Copper	3	0.23	2×10^8	3	6.4
Aluminum	2	0.1	1.6×10^8	1.5	2.7
Gallium	3	0.21	3.3×10^5	2.5	2.5
Nickel	3	0.47	1.5×10^7	3	7.2

mode of heat transfer and the medium is radiatively nonparticipating. Case 2 is equivalent to an isothermal furnace. In all calculations a sound pressure level (SPL) of 160 dB, required to levitate a droplet of water in air at room temperature,[12] is used as reference. The acoustic forces for liquid metals can be as much as 12 times greater than that for water, as shown in Table 2.

For the combined acoustic-electromagnetic case, the interface condition is

$$\gamma K + P_m + P_s = 0 \tag{15}$$

Thus, for the combined case, in the most conservative estimate, Eq. (15) implies that the effective pressure at the interface is $(P_s - P_m)$. The application of this result is explained for the case of copper (row 1 of Table 2). Since P_m is of the order of the levitating pressure, and $P_s \approx 3P_{s,\text{ref}}$ is the acoustic levitating pressure, it follows that $P_m \approx 3P_{s,\text{ref}}$. The acoustic driving pressure now becomes, from Eq. (15), $4.5P_{s,\text{ref}}$ in order to keep the effective interface pressure at $1.5P_{s,\text{ref}}$. Thus, to order of magnitude, the acoustic driving force in the presence of an electromagnetic field is just a sum of the driving and levitating forces for the purely acoustic cases.

Table 3 is a list of some of the requirements for systems in microgravity. The driving forces do not change since they are independent of gravitational acceleration (and are dependent on the surface tension). The levitating forces, as Table 3 reveals, are at least three orders of magnitude lower than in Earth's gravity. The heating time is very large for a minimum B. This suggests that it may be necessary to increase either B, or the frequency, to obtain better heating.

The analysis of this work indicates that a combination of the electromagnetic and acoustic forces is feasible. In Earth-based experiments, the requirements are higher than in the low-temperature acoustic applications. In microgravity, however, the results are highly encouraging, since very minimal forces are required, and the equilibrium shapes are more nearly spherical. In addition, radiation is the dominant mode of heat transfer under microgravity conditions, and since the inert atmospheres usually used in these applications do not participate significantly, the assumption of negligible temperature gradient is less restrictive.

Acknowledgments

The authors wish to acknowledge the partial support by the Houston Area Research Center and the stimulating discussions with John Margrave and Shankar Krishnan.

References

[1]Barmatz, M., "Overview of Containerless Processing Technologies," *Materials Processing in the Reduced Gravity Environment of Space*, edited by G.E. Rindone, North Holland, Amsterdam, 1982, pp. 25-37.

[2]Apfel, R. E., "Technique for Measuring Adiabatic Compressibility, Density, and Sound Speed of Submicroliter Liquid Samples," *Journal of the Acoustical Society of America*, Vol. 59, Feb. 1976, pp. 339-343.

[3]Trinh, E. H., "Compact Acoustic Levitation Device for Studies in Fluid Dynamics and Material Science in the Laboratory and Microgravity," *Review of Scientific Instruments*, Vol. 56, Nov. 1985, pp. 2059-2065.

[4]Okress, E. C., Wroughton, D. M., Comenetz, G., Brace, P. H., and Kelley, J. C. R., "Electromagnetic Levitation of Solid and Molten Metals," *Journal of Applied Physics*, Vol. 23, May 1952, pp. 545-552.

[5]Krishnan, S., Hansen, G. P., Hauge, R. H., and Margrave, J. L., "Observations on the Dynamics of Electromagnetically Levitated Liquid Metals and Alloys at Elevated Temperatures," *Metallurgical Transactions A*, Vol. 19A, Aug. 1988, pp. 1939-1943.

[6]Mestel, A. J., "Magnetic Levitation of Liquid Metals," *Journal of Fluid Mechanics*, Vol. 117, 1982, pp. 27-43.

[7]Sneyd, A. D. and Moffatt, H. K., "Fluid Dynamical Aspects of the Levitation Melting Process," *Journal of Fluid Mechanics*, 1982, Vol. 117, pp. 45-70.

[8]El-Kaddah, N. and Szekely, J., "Electromagnetic Force Field, Fluid Flow Field and Temperature Profiles of Levitated Metal Droplets," *Metallurgical Transactions B.*, Vol. 14B, Sept. 1983, pp. 401-409.

[9]Margrave, J. L., "Heat Capacities of Liquid Metals over 1500 K," *Materials Processing in the Reduced Gravity Environment of Space*, edited by G. E. Rindone, North Holland, Amsterdam, 1982, pp. 39-42.

[10]Shimoji, M., *Liquid Metals*, Academic Press, London, 1977.

[11]Marston, P. L., "Shape Oscillations and Static Shape Deformation of Drops and Bubbles Driven by Modulated Radiation Stresses – Theory," *Journal of the Acoustical Society of America*, Vol. 67, Jan. 1980, pp. 15-26.

[12]Trinh, E. H., and Hsu, C-J., "Equilibrium Shapes of Acoustically Levitated Drops," *Journal of the Acoustical Society of America*, Vol. 79, May 1986, pp. 1135-1138.

CO_2 Laser Absorption in SF_6-Air Boundary Layers

H. F. Nelson*
University of Missouri—Rolla, Rolla, Missouri
and
E. A. Eiswirth†
McDonnell Douglas, St. Louis, Missouri

Introduction

GASEOUS sulfur hexafluoride (SF_6), which absorbs radiation at 10.6 μm, can be injected into boundary

Received June 17, 1988; revision received July 15, 1988.

*Professor of Aerospace Engineering, Thermal Radiative Transfer Group, Department of Mechanical and Aerospace Engineering. Associate Fellow AIAA.

†Section Chief-Aeromechanics. Senior Member AIAA.

layers to attenuate radiation. This concept potentially can protect aircraft and missile surfaces from CO_2 laser beams. The SF_6 absorption decreases for increasing temperature and becomes very small above 570°K. Since the absorbed energy increases local temperature, the boundary layer can become transparent to CO_2 lasers.

The computer code, INJECT, predicts boundary-layer profiles, including slot injection of a foreign gas.[1-3] It solves the supersonic, turbulent, nonsimilar boundary-layer equations using a finite-difference method. INJECT has been modified to account for laser radiation absorption. This note describes an investigation of CO_2 laser absorption by SF_6 in planar, turbulent boundary layers.

Radiative Transfer Equation

The laser beam intensity in a boundary layer, assuming steady-state, one-dimensional radiative transfer with no emission and scattering, is

$$I(\tau) = I_o\delta(\mu - 1)\delta(\phi - 0)\exp(\tau - \tau_o) \qquad (1)$$

where $\tau = \int_o^y \alpha(y')\,dy'$, $\tau_o = \int_o^\delta \alpha(y')\,dy'$, α is the absorption coefficient per unit length, I_o is the laser radiation incident at the edge of the boundary layer $y = \delta$, δ is the boundary-layer thickness at position x, and the wavelength dependence of I and α has been neglected because laser radiation is being considered. The Dirac delta-function product restricts the laser to the normal direction. The variables τ and τ_o represent the optical depth at the location where I is calculated and the maximum optical thickness of the boundary layer, respectively.

For the intensity distribution of Eq. (1), the radiative flux is

$$q_R(\tau) = \int_o^{2\pi}\int_o^1 I(\tau)\mu\,d\mu\,d\phi = I_o\exp(\tau - \tau_o) \qquad (2)$$

and the magnitude of the flux at $\tau = \tau_o$ is I_o. The quantity $\partial q_R/\partial y$ is the radiation term in the energy equation.[4] It can be written as $-\alpha I$ from Eq. (2), in agreement with Anderson.[5-7] The radiative absorption coefficient for SF_6 is

$$\alpha = P_{SF_6}(564 - 0.985T)\ 1/\text{cm}, \qquad \text{for } T \le 570°\text{K}$$
$$\alpha = 0 \qquad \text{for } T > 570°\text{K} \qquad (3)$$

where P_{SF_6} is the partial pressure of SF_6 in atmospheres and T is the temperature in °K.[6]

Results and Discussion

Calculations are presented for Mach 3 flow over an adiabatic flat plate, as shown schematically in Fig. 1. The CO_2 laser beam was assumed to have a uniform intensity distribution and a flux of 5 kW/cm^2. SF_6 was injected tangentially through a 0.0635-cm-high slot into the base of the boundary layer. As the SF_6 absorbs the laser energy, its temperature increases, which in turn influences the velocity, composition, and enthalpy profiles across the boundary layer. The slot was 69.29 cm downstream of the leading edge, where the Reynolds number based on x was 2.57×10^8 and the boundary-layer thickness was 1.13 cm. The slot had a 0.0254-cm lip. The flow of SF_6 was laminar, sonic, and fully developed at the slot exit. Additional details of the flowfield are given in Table 1. Boundary-layer profiles are presented at streamwise positions corresponding to the nearside ($x/s = 0.80$), middle (5.88), and far side (10.96) of the laser beam, where s is the slot height (0.0635 cm).

Figure 2 shows temperature profiles for $q_R(\delta) = 0$ and 5 kW/cm^2. The radiation-free temperature profile at $x/s = 0.80$ has a step-like decrease from the SF_6 flow to the airflow. Downstream, the effects of turbulent mixing erode the step change.

When $q_R(\delta) = 5$ kW/cm^2, the absorption of laser energy distorts the temperature profiles so that the maximum temper-

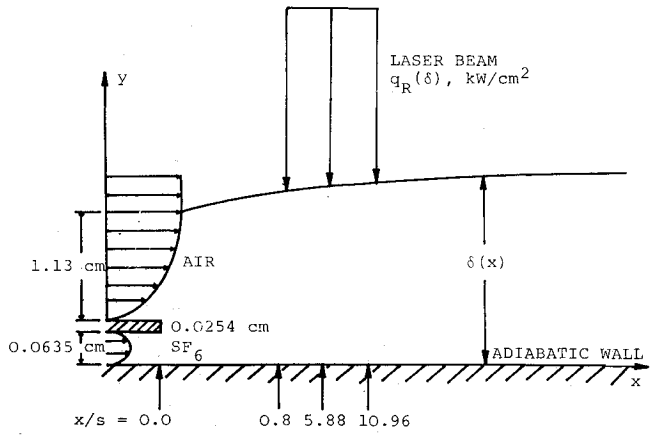

Fig. 1 Schematic of the boundary-layer/laser interaction problem. The laser is assumed to have a uniform intensity distribution.

Table 1 Flowfield conditions

	Air freestream	SF_6 slot exit
Mach number	3	1
Static pressure (atm)	1.08	1.08
Static temperature (°K)	90.7	293.3
Total temperature (°K)	254.4	302.8
Mass flow rate (g/cm^2/s)	22.35	4.15

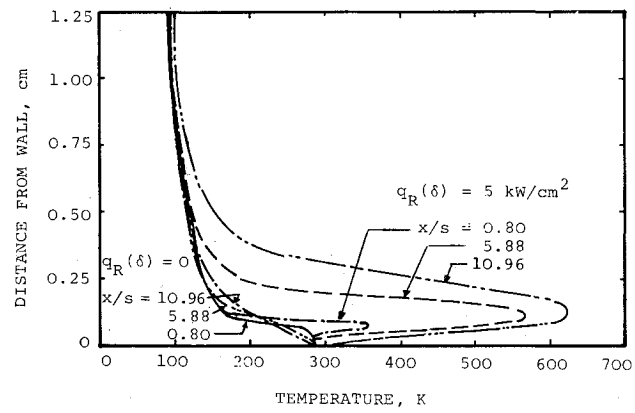

Fig. 2 Effect of laser energy absorption on boundary-layer temperature profiles at $x/s = 0.80$, 5.88, and 10.96.

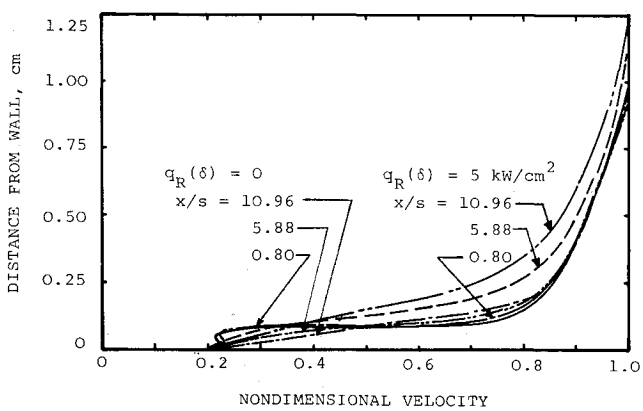

Fig. 3 Effect of laser energy absorption on boundary-layer velocity profiles at $x/s = 0.80$, 5.88, and 10.96.

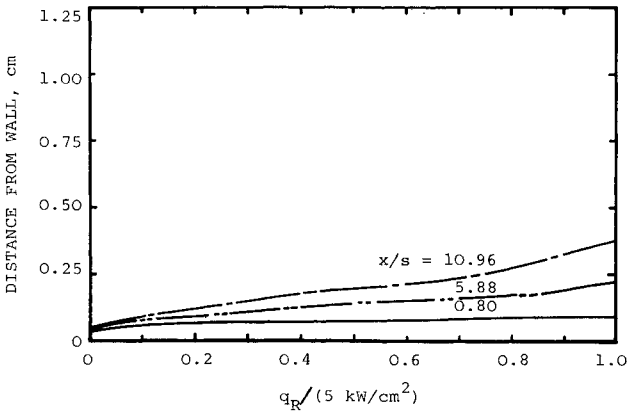

Fig. 4 Laser radiation profile in the boundary layer as a function of position along the flat plate.

ature occurs in the mixing layer between the air and the SF_6. The magnitude of the maximum temperature increases in the streamwise direction across the laser beam because the gas has absorbed more laser energy. At the far side of the laser beam, the temperature becomes so high that the SF_6 absorption coefficient is zero in part of the mixing layer (saturation). Consequently, radiation is absorbed above and below the high-temperature layer. This causes the adjacent gas to become hotter and the thickness of the high temperature layer to increase. The absorption of laser radiation and its subsequent heating increase the thermal boundary-layer thickness. SF_6 is dispersed farther into the airflow as the SF_6 is heated.

Figure 3 shows velocity profiles for $q_R(\delta) = 0$ and 5 kW/cm^2. At $x/s = 0.80$ for $q_R(\delta) = 0$, the velocity profile has a steplike jump in the mixing layer between the SF_6 and air, and the wake from the slot lip is evident. The velocities rapidly diffuse into a continuous profile downstream. Also, the boundary-layer thickness does not change very much with streamwise position for $q_R(\delta) = 0$.

When $q_R(\delta) = 5$ kW/cm^2, the boundary layer becomes thicker and the velocity profiles become smoother. The laser does not influence the velocity profile very much at $x/s = 0.80$. Further downstream, the absorption of laser energy reduces the air-side mixing layer velocity, because the slower moving SF_6 diffuses rapidly into the air since its temperature is higher. These effects reduce the velocity and increase the boundary-layer thickness.

The absorption coefficient of SF_6 increases as the partial pressure of SF_6 increases. Absorption of laser energy increases not only the temperature but also the partial pressure of SF_6 throughout the mixing layer relative to its value for $q_R(\delta) = 0$. Therefore, the temperature in the mixing layer is high compared to the temperature in the gas above and below it. The coupled increase of temperature and pressure causes the optical thickness of the boundary layer to increase when laser energy is absorbed.

Figure 4 shows the nondimensional laser flux $q_R/q_R(\delta)$ where $q_R(\delta) = 5$ kW/cm^2 as a function of distance across the boundary layer at three streamwise positions. Laser radiation does not reach the wall at any of the streamwise positions. The rapid diffusion of SF_6 into air is responsible for the reduction of the laser intensity further from the wall for increasing streamwise positions. At $x/s = 0.80$, the radiation penetrates much deeper into the boundary layer before it begins to be absorbed compared with $x/s = 10.96$.

Conclusions

Injection of SF_6 into the boundary layer is an effective way to absorb CO_2 laser radiation and to protect aerodynamic surfaces from CO_2 laser beams. The strong temperature dependence of the SF_6 absorption coefficient makes the boundary layer become transparent to the CO_2 laser radiation when the SF_6 temperature becomes greater than about 570°K. The absorbed energy couples strongly into the velocity, enthalpy, temperature, and composition profiles across the boundary layer. The energy absorption increases the diffusion rate of the SF_6 in the boundary layer.

References

[1]Hixson, B. A., Beckwith, I. E., and Bushnell, D. M., "Computer Program for Compressible Laminar or Turbulent Nonsimilar Boundary Layers," NASA TM X2140, April 1971.

[2]Beckwith, I. E. and Bushnell, D. M., "Calculation by a Finite-Difference Method of Supersonic Turbulent Boundary Layers with Tangential Slot Injection," NASA TN D-6221, April 1971.

[3]Cary, A. M., Bushnell, D. M., and Hefner, J. N., "Calculation of Turbulent Boundary Layers with Tangential Slot Injection," American Society of Mechanical Engineers Paper 77-WA/HT-27, Nov. 1977.

[4]Vincenti, W. G. and Kruger, C. H., *Introduction to Physical Gas Dynamics*, Wiley, New York, 1965, Chap. 12.

[5]Anderson, J. D., "A Numerical Analysis of CO_2 Laser Radiation Absorption in SF_6-Air Laminar Boundary Layers," Naval Ordnance Laboratory, Silver Spring, MD, NOLTR 73-143, July 1973.

[6]Anderson, J. D., "Computations of CO_2 Laser Radiation Absorption in SF_6-Air Boundary Layers," *AIAA Journal*, Vol. 12, Nov, 1974, pp. 1527–1533.

[7]Wagner, J. L. and Anderson, J. D., "Laser Radiation-Gasdynamic Coupling in the SF_6-Air Laminar Boundary Layer," *AIAA Journal*, Vol. 18, March 1980, pp. 333–334.

Melting of a Semitransparent Polymer Under Cyclic Constant Axial Stress

I. S. Habib*
University of Michigan—Dearborn, Dearborn, Michigan

Nomenclature

A_r = a constant related to the effect of temperature on viscosity
c = specific heat capacity
k = thermal conductivity of the solid
L = slab half-thickness
N_r = radiative conductive number = $(n^2\sigma T_1^3 L)/k$
N_s = inverse of Stefan number = $\lambda/T_1 c$
n = material index of refraction
q_r = radiative heat flux; $q_r^* = q_r/(n^2\sigma T_1^4)$
s = thickness of the solid phase; $s^* = s/L$
T = temperature; T_1 = cold boundary temperature; T_m = melt temperature
t = time; t also = dummy integration variable; $t^* = t\alpha/L^2$
x = distance from cold boundary
α = thermal diffusivity
β = heat generation parameter = $A_r \gamma L^2/k$; β_c = critical value of β
γ = heat generation per unit volume
δ = $A_r T_1$
κ = absorption coefficient
λ = latent heat of melting

Presented as Paper 87-1492 at the AIAA 22nd Thermophysics Conference, Honolulu, HI, June 8–10, 1987; received June 22, 1987; revision received March 21, 1988.

*Professor of Mechanical Engineering.